Fabrication of Functional Organic-Inorganic Hybrid Materials using Mesoporous Silica

（メソポーラスシリカを利用した機能性有機／無機ハイブリッドマテリアルの創製）

リンタング　ヘンドリック オクテンディー

Introduction

Organic-inorganic hybrid materials have attracted attention, since desired functions can be tailored by organic motifs, while their organic assembled structures can be immobilized by inorganic frameworks.[1] For immobilization, silicate nanochannels of mesoporous silica have often been used, where certain performances of organic motifs can be enhanced due to site isolation or long-range molecular ordering.[2] Since the pioneering work by us[3a] and other groups[3b, 3c] in 2001, we have demonstrated so far that, by using functional amphiphiles as templates for the sol-gel synthesis of organic/silica nanocomposites, a variety of organic functionalities can be incorporated into silicate nanochannels. On the other hand, we have also reported that hydrophobic trinuclear dendritic pyrazolate complexes of Au(I), Ag(I), and Cu(I), self-assembled into columnar aggregates through metallophilic interactions, forming photoluminescent superhelical fiber[4a] and phosphorescent organogels[4b], which are applicable to the fabrication of rewritable phosphorescent papers.[4c]

My research subject focuses on utilization of an amphiphilic version of the cylindrical assembly of trinuclear Au(I) pyrazolate complex as a template for the sol-gel synthesis of novel phosphorescent mesostructured silica composites. New functional organic-inorganic hybrid materials, such as 1) self-repairable optoelectronic nanostructured materials and 2) metal ion permeation in congested hexagonal silicate nanochannels, could be developed by using these organometallic/silica nanocomposites.

Results and Discussion

1. Encouraged Self-Repairing of 1D Molecular Assembly in Mesoporous Silica by a ‘Nanoscopic Inorganic Template’

Mesostructured silica film composite with a hexagonal geometry **Au_3Pz_3/$Silica_{hex}$** (Figure 1b), was successfully synthesized by using the amphiphilic trinuclear Au(I) pyrazolate complex **Au_3Pz_3** (Figure 1a) as a template for the sol-gel synthesis with tetrabutoxysilane (TBOS). Typically, an acidic aqueous EtOH solution (EtOH, 29 mg, 0.6 mmol; HCl, 12 N, 0.15 mg, 1.5 x 10^{-3} mmol; H_2O, 6 mg, 0.3 mmol) of a mixture of **Au_3Pz_3** (5 mg, 1.25 x 10^{-3} mmol) and TBOS (24 mg, 74.9 x 10^{-3} mmol) was kept for 12 h at room temperature ([**Au_3Pz_3**]/[TBOS]/[EtOH]/[HCl]/[H_2O] =

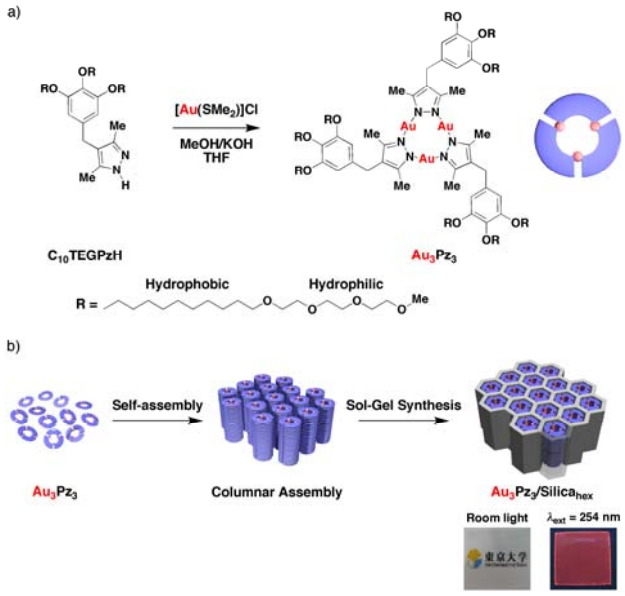

Figure 1. a) Synthesis and molecular structure of **Au_3Pz_3**. b) Sol-gel synthesis of mesostructured silica **Au_3Pz_3/$Silica_{hex}$** with a hexagonal geometry templated by columnarly assembled **Au_3Pz_3**. Photographs were taken at room temperature under room light (lower left) and on exposure to a 254 nm ultraviolet light (lower right).

1/60/504/1.2/266), where partial oligomerization of TBOS took place. The resulting viscous solution (20 μL) was spin-coated on a quartz plate at 3000 rpm for 15 s, affording a colorless transparent film (Figure 1b, inset), which was dried in air for 24 h at room temperature and then additional 12 h at 40 °C. The powdered sample of **Au_3Pz_3/Silica$_{hex}$** obtained by scratching the spin-coated film displayed X-ray diffraction (XRD) peaks at 2θ = 2.16°, 3.70º, and 4.30°, which can be indexed as d_{100}, d_{110}, and d_{200}, respectively, of a hexagonal structure with an interpore distance of 4.1 nm (Figure 2a (B)). The absence of the peak due to d_{110} for the as-prepared film of **Au_3Pz_3/Silica$_{hex}$** suggests that the c-axis of the hexagonal unit cell is oriented parallel to the quartz surface (Figure 2a (A)). Transmission electron microscopy (TEM) of the cross-section of the spin-coated film allowed for visualization of the hexagonal geometry of the silicate framework (Figure 3). Noteworthy, when the molar ratio of TBOS to **Au_3Pz_3** was changed from 60:1 to 20:1 (8 mg, 25 x 10^{-3} mmol), a lamellar structure with an interlayer distance of 3.7 nm formed (Figures 2b (A) and B) of the spin-coated film (**Au_3Pz_3/Silica$_{lam}$**).

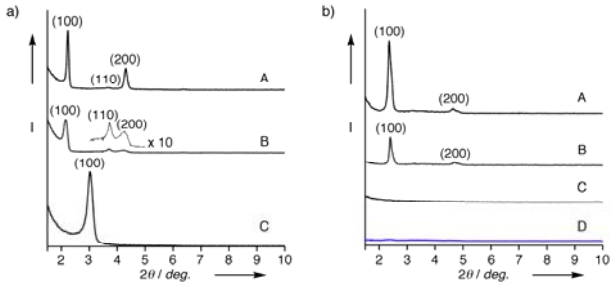

Figure 2. X-ray diffraction patterns of a) **Au_3Pz_3/Silica$_{hex}$** and b) **Au_3Pz_3/Silica$_{lam}$**. (A) as-synthesized spin-coated films and (B) powder samples obtained by scratching off the spin-coated films, (C) spin-coated films after calcination at 450 °C for 3 h, and (D) a spin-coated film (**Au_3Pz_3/Silica$_{lam}$**) after heating at 140 °C for 10 min (blue curve).

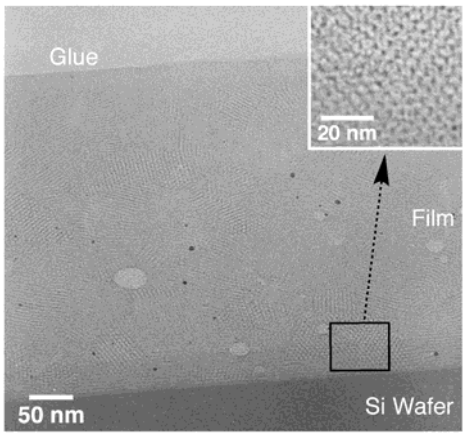

Figure 3. TEM micrograph of an as-synthesized spin-coated film of **Au_3Pz_3/Silica$_{hex}$** (cross section).

On exposure to 254 nm UV light with a hand-held lamp, **Au_3Pz_3/Silica$_{hex}$** with a hexagonal geometry emitted in red (Figure 1b, inset) with a luminescence center (λ_{em}) at 693 nm (Figure 4b). Monitoring the emission at 693 nm provided an excitation spectrum with a peak maximum at 276 nm (Figure 4a), indicating that this red luminescence has a very large Stokes shift ($\Delta\lambda$ = 417 nm). Also noteworthy is a long lifetime (τ_{20} = 7.8 μs) of this luminescence, evaluated at 20 °C by means of transient emission spectroscopy upon laser excitation at 266 nm. These spectral features are characteristic of phosphorescing events from metal-centered triplet excited states modified with a Au(I)–Au(I) metallophilic interaction. Quite analogous phosphorescence properties were observed for a bulk material of assembled **Au_3Pz_3** (λ_{em} = 690 nm, τ_{20} = 6.3 μs) and silica composite **Au_3Pz_3/Silica$_{lam}$** with a lamellar geometry (λ_{em} = 690 nm, τ_{20} = 6.7 μs), indicating that the photochemical properties of assembled **Au_3Pz_3** in the solid state are essentially maintained to the hybridization with silica.

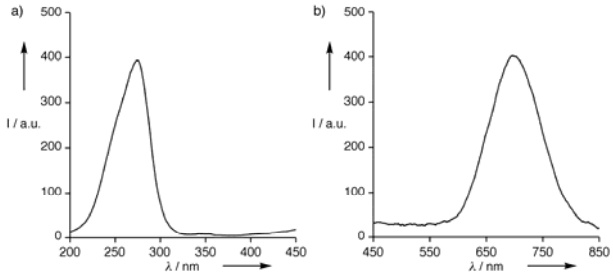

Figure 4. a) Excitation (λ_{em} = 693 nm) and b) emission (λ_{ext} = 276 nm) spectra of **Au_3Pz_3/Silica$_{hex}$** at 20 °C.

The bulk material of assembled **Au_3Pz_3** became less emissive upon heating (Figure 5a, red). For example, when this material was stepwise heated from 20 to 40, 80, 120 and 140 °C, its phosphorescence was progressively less intensified to 41, 20, 12 and 9%, respectively, of the original intensity (Figure 5a, red). Likewise, a thin film of mesostructured silica composite

Au_3Pz_3/Silica$_{hex}$ with a hexagonal geometry showed lower emission capabilities at higher temperatures (Figure 5a, gray). However, this nanocomposite material showed a much smaller temperature dependency than bulk **Au_3Pz_3**. For example, upon heating to 80 and 120 °C, **Au_3Pz_3/Silica$_{hex}$** retained even 77 and 56% of its original luminescence intensity, respectively (Figure 5a, gray). Such a heat-resistant phosphorescing capability is quite advantageous for many practical applications. Although the light-emitting capability of silica composite **Au_3Pz_3/Silica$_{lam}$** with a lamellar geometry showed a better heat resistivity (Figure 5a, green) than that of bulk **Au_3Pz_3** (Figure 5a, red), is was obviously inferior to that of **Au_3Pz_3/Silica$_{hex}$** adopting a hexagonal geometry (Figure 5a, gray).

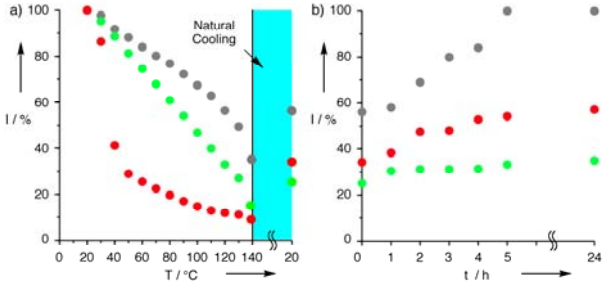

Figure 5. Changes in a), b) emission intensities (normalized) at 693 nm (λ_{ext} = 276 nm) of **Au_3Pz_3/Silica$_{hex}$** (gray), **Au_3Pz_3/Silica$_{lam}$** (green), and bulk **Au_3Pz_3** (red) on a) stepwise heating from 20 to 140 °C followed by natural cooling from 140 to 20 °C and b) being kept at 20 °C for 24 h after natural cooling from 140 °C.

If the observed luminescence loss upon heating is induced only by thermal quenching of the photoexcited state, lowering the temperature could coincidentally result in complete restoration of the original luminescence intensity. However, all of these materials, on cooling from 140 to 20 °C, displayed only a partial recovery of the luminescence intensity (Figure 5a, blue bar area): 9 → 35% for **Au_3Pz_3** (red), 35 → 56% for **Au_3Pz_3/Silica$_{hex}$** (gray), and 15 → 25% for **Au_3Pz_3/Silica$_{lam}$** (green). Therefore, it is likely that the luminescence loss upon heating is more or less caused by a thermally induced structural damage of cylindrical assembly of **Au_3Pz_3**.

For the contrasting heat-resistivities of the luminescence properties of **Au_3Pz_3/Silica$_{hex}$** and **Au_3Pz_3/Silica$_{lam}$**, I wondered if the hexagonal and lamellar silicate frameworks inherently possess different thermal stabilities from one another. Upon calcination of **Au_3Pz_3/Silica$_{hex}$** at 450 °C for 3 h, the calcined film of **Au_3Pz_3/Silica$_{hex}$** still showed a diffraction pattern consistent with a hexagonal geometry (Figure 2a (C)), whilst the observed 2θ values (2.90° and 5.00°) indicate reduction of the interpore distance from 4.1 to 2.9 nm. In sharp contrast, **Au_3Pz_3/Silica$_{lam}$** was completely disrupted to lose its lamellar structure (Figure 2b (C)). To my surprise, such a structural disruption also took place even when **Au_3Pz_3/Silica$_{lam}$** was heated to 140 °C, where the XRD profile became totally silent within only 10 min (Figure 2b (D)). This observation suggests the crashed silicate layers hamper reconstruction of the elaborate molecular geometry for light emission.

I noticed that the bulk material of assembled **Au_3Pz_3**, when allowed to stand at 20 °C after being heated to 140 °C, gradually retrieves the luminescence intensity (Figure 5a, red) due to a dynamic nature of the metallophilic interaction. However, this event was subsided in 4 h, to furnish only a 35 → 54% recovery of its original intensity (Figure 5b, red). To my surprise, in the case of mesostructured silica composite **Au_3Pz_3/Silica$_{hex}$**, where the luminescent cylindrical assembly of **Au_3Pz_3** is confined in the silicate nanochannels, perfect restoration of the phosphorescence intensity took place (Figure 5a, gray). Under identical conditions to those for bulk **Au_3Pz_3**, the phosphorescence of **Au_3Pz_3/Silica$_{hex}$** was recovered only in the initial 3 h from 56 to 80% of its original intensity and then further to 100% after 5 h (Figure 5b, gray). This autonomous recovery

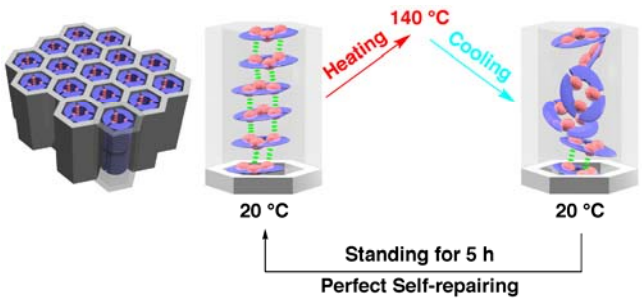

Figure 6. Self-repairing capabilities of columnarly assembled **Au_3Pz_3** immobilized within hexagonal silicate nanochannels (**Au_3Pz_3/Silica$_{hex}$**).

indicates the occurrence of complete reconstruction of cylindrically assembled **Au_3Pz_3** in the confined silicate nanochannels from heat-induced structural damages (Figure 6). The self-repairing nature, thus observed for **Au_3Pz_3/$Silica_{hex}$** (Figure 5b, gray) can be referred to as 'nanoscopic template effect' (Figure 6). Of further interest, silica composite **Au_3Pz_3/$Silica_{lam}$** with a lamellar geometry, in contrast, displayed a very poor self-restoration profile at 20 °C (Figure 5a, green), allowing, even after 24 h, only 35% recovery of its original luminescence intensity (Figure 5b, green). Namely, the lamellar silicate gives rise to a negative effect on the reconstruction of the luminescent geometry.

2. Metal Ion Permeation in Congested Nanochannels: Exposure Effect of Ag^+ on Phosphorescent Properties of a Gold Pyrazolate Complex Immobilized in the Nanoscopic Channels of Mesoporous Silica

When mesostructured silica film composite with a hexagonal geometry **Au_3Pz_3/$Silica_{hex}$** (Figure 1b) was dipped at 20 °C into THF solutions of 100 /M AgOTf, the resulting material **Ag@Au_3Pz_3/$Silica_{hex}$** (Figure 7) upon excitation at 276 nm showed new emission band at 486 nm (Figures 8a and 8b) characteristic of a Au(I)-Ag(I) heterometallic interaction,[5b] in addition to the less-intensified original phosphorescence band at 693 nm. On exposure to 254 nm UV light with a hand-held lamp, **Ag@Au_3Pz_3/$Silica_{hex}$** emitted in green (Figure 7, inset) with a luminescence center at 486 nm (Figures 8a and 8b). The decrease in the intensity of 693 nm-emission band subsided at 18% of the original intensity in 60 min when concentration of AgOTf was 100 /M (Figure 8a, inset), while 10 /M AgOTf (Figure 8b, inset) resulted in smaller and slower spectral changes (41% of the original intensity in 120 min). These observations suggest incorporation of Ag^+ into open pore of the hexagonal silicate nanochannels of **Au_3Pz_3/$Silica_{hex}$** including the cylindrical assembly of **Au_3Pz_3**.

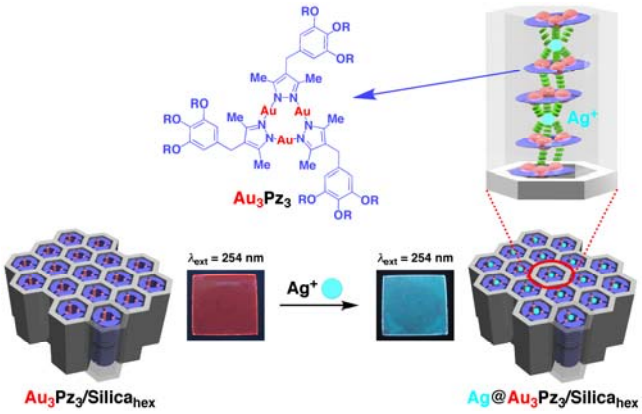

Figure 7. Phosphorescence color change of the film of **Au_3Pz_3/$Silica_{hex}$** caused by dipping into a THF solution of 100 /M AgOTf for 60 min at 20 ºC. Photographs were taken on exposure to ultraviolet light a 254 nm.

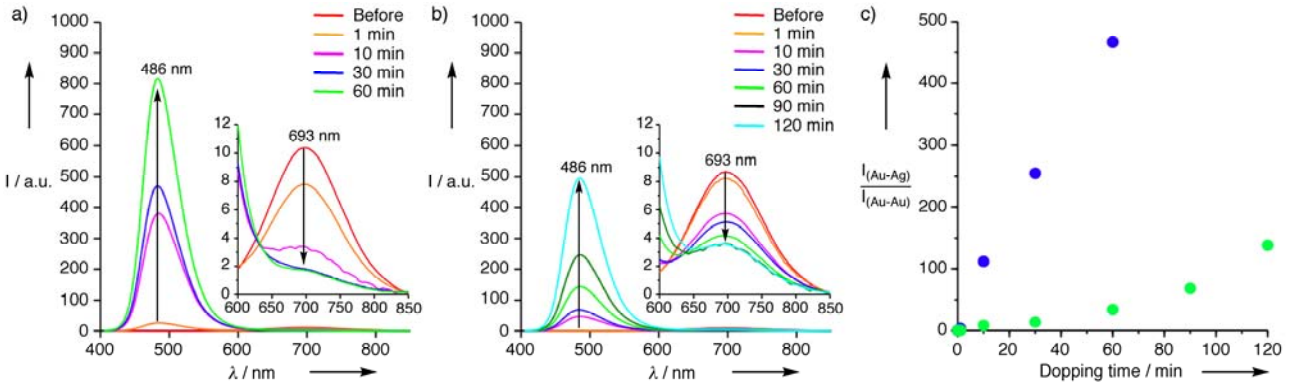

Figure 8. Emission (λ_{ext} = 276 nm) spectral changes of a film of **Au_3Pz_3/$Silica_{hex}$** at 20 °C before and after dipping into a THF solution of a) 100 and b) 10 /M AgOTf. c) Changes in emission intensities (λ_{ext} = 276 nm) of a film of **Au_3Pz_3/$Silica_{hex}$** due to Au(I)–Ag(I) and Au(I)–Au(I) metallophilic interactions at 486 and 693 nm, respectively, after dipping into THF solutions of 100 (blue) and 10 /M (green) AgOTf.

Ag^+ and cylindrically assembled trinuclear Au(I) complex can form a sandwich adduct in solid state.[5] In soft materials, the columnar assembly of Au(I) or Cu(I) pyrazolate complexes afforded reversible phosphorescent color switching properties in response to external stimuli such as heat and Ag^+.[4b] I then attempted the sol-gel synthesis of mesoporous silica with **Au_3Pz_3** as a template in the presence of Ag^+ (Figure 9). A typical procedure for the fabrication of mesostructured silica **Ag@Au_3Pz_3/$Silica_{hex}$** is as follows: a THF solution of AgOTf (2.5 μL) was added to **Au_3Pz_3** (10 mg, 2.5 x 10^{-3} mmol) in THF (200 μL), and the mixture was evaporated to leave a green residue, which was then dissolved in an acidic aqueous EtOH solution (EtOH, 58 mg, 1.2 mmol; HNO_3, 16 N, 0.44 mg, 4.6 x 10^{-3} mmol; H_2O, 12 mg, 0.6 mmol). TBOS (48 mg, 150 x 10^{-3} mmol) was added to this solution, and the mixture was kept for 12 h at room temperature, where partial oligomerization of TBOS took place. The resulting viscous solution (20 μL) was spin-coated on a quartz plate at 3000 rpm for 15 s, affording a colorless transparent film, which was dried in air for 24 h at room temperature. According to the increment in the molar ratio of AgOTf to **Au_3Pz_3** in the sol-gel synthesis, the ratio of the emission intensity at 486 nm due to Au(I)–Ag(I) to that at 693 nm due to Au(I)–Au(I) of **Au_3Pz_3/$Silica_{hex}$** was progressively increased (Figure 10). It is noteworthy that the amounts of Ag^+ taken into the film of **Au_3Pz_3/$Silica_{hex}$** by dipping into THF solutions of 100 and 10 μM AgOTf for 60 min are estimated to be 11 and 9% (corresponding to the atomic ratios of Au to Ag = 2.8 : 1 and 3.5 : 1), respectively, based on the plots in Figure 10.

Figure 9. Schematic illustration of the sol-gel synthesis of hexagonal mesostructured silica **Ag@Au_3Pz_3/$Silica_{hex}$** templated by 1D columnar assembly of **Au_3Pz_3** in the presence of Ag^+.

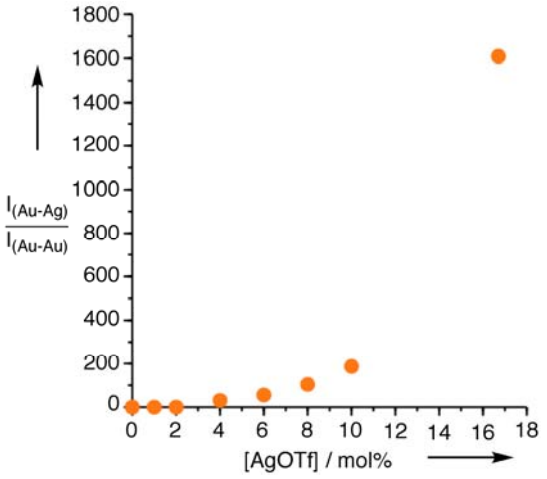

Figure 10. Changes in relative emission intensities ratio (λ_{ext} = 276 nm) of Au(I)–Ag(I) (λ_{em} = 486 nm) and Au(I)–Au(I) (λ_{em} = 693 nm) for a film of **Ag@Au_3Pz_3/$Silica_{hex}$** prepared by the sol-gel synthesis with different molar ratios AgOTf to **Au_3Pz_3** (0.0, 1.0, 2.0, 4.0, 6.0, 8.0, 10.0, and 16.7%)

The excitation spectrum of the film of **Au_3Pz_3/$Silica_{hex}$** for 693 nm emission showed a peak maximum at 276 nm, which was less-intensified upon dipping the film into THF solutions of AgOTf (Figure 8a). On the other hand, the excitation spectra for 486 nm emission showed a peak maximum at 276 nm with a small peak at 390 nm, where the intensity of these two peaks are simultaneously intensified upon dipping. Upon excitation at 396 nm, the resulting **Ag@Au_3Pz_3/$Silica_{hex}$** displayed a single luminescence center at 486 nm, while excitation at 276 nm results in emissions at both 486 and 693 nm. It should be noted here that comparison of the emission spectra after dipping for 30 and 60 min show that the emission due to Au(I)–Au(I) metallophilic interaction is mostly lost in both spectra while that due to Au(I)–Ag(I) heterometallic interaction drastically intensified from 30 to 60 min. This observation suggests that the emission due to Au(I)–Au(I) metallophilic interaction (693 nm) is quenched in part in **Ag@Au_3Pz_3/$Silica_{hex}$**, and that the new emission at 486 nm was intensified upon conversion of the Au(I)–Au(I) metallophilic interaction to the Au(I)–Ag(I) heterometallic interaction. Namely, upon photoexcitation at 276 nm, an energy transfer from the excited Au(I)–Au(I) species to Au(I)–Ag(I) species likely takes place in **Ag@Au_3Pz_3/$Silica_{hex}$**.

X-ray photoelectron spectroscopy (XPS) of **Au_3Pz_3/$Silica_{hex}$** film allows us to evaluate the ratio of Au to Ag from the intensities of Au 4f (84.3 and 88.1 eV) and Ag 3d (368.1 and 374.1 eV) XPS

peaks. Actually, after dipping into a THF solution of 100 /M AgOTf for 60 min, the atomic ratio of Au to Ag was evaluated to be 3:7, at surface. Depth profiling experiments using an argon ion etcher with a 500 V accelerated voltage showed that, after sputtering for 5, 15, 30 and 75 s, the atomic ratios of Au to Ag changed to 2:3, 3:2, 2.3:1 and 3:1, respectively (Figures 11a and 11b). After sputtering for 115 s and 195 s, the peaks due to Ag 3d and Au 4f were sequentially disappeared, respectively. These results strongly suggest that the color change observed upon dipping the film of **Au_3Pz_3/$Silica_{hex}$** into a THF solution of Ag^+ does not originate from the adsorption of Ag^+ on the surface, but is due to permeation of Ag^+ into the nanochannel of **Au_3Pz_3/$Silica_{hex}$** to form heterometallic composite **Ag@Au_3Pz_3/$Silica_{hex}$** (Figure 1).

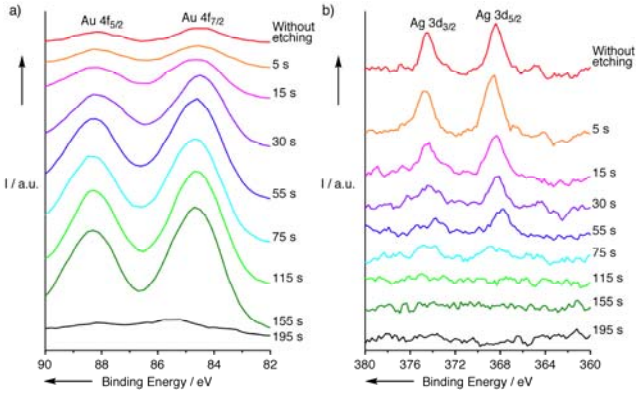

Figure 11. Changes in XPS spectra of **Au_3Pz_3/$Silica_{hex}$** after dipping into a THF solution of 100 /M AgOTf for 60 min upon sputtering for 5, 15, 30, 55, 75, 115, 155, and 195 s. a) Au 4f and b) Ag 3d regions.

Conclusions

I have demonstrated the first successful fabrication of organic-inorganic nanostructured composites using mesoporous silica with a hexagonal geometry as a framework and a luminescent cylindrically assembled metal pyrazolate complex as a template for the sol-gel synthesis. New functional organic-inorganic hybrid materials can be developed by using these phosphorescent nanocomposites such as 1) self-repairable optoelectronic nanomaterials that recovers from structural damages caused by heating due to 'nanoscopic template effect' and 2) exposure effect on phosphorescent properties from red to green due to metal ion permeation in congested hexagonal silicate nanochannels. These works may shed light on a general issue of how one can ensure the high reliability of molecular devices for long-term operation and the high sensitivity of composite materials for metal ion and gas sensors.

References

1. C. Sanchez, B. Julián, P. Belleville, M. Popall, *J. Mater. Chem*. **2005**, *15*, 3559–3592.
2. F. Hoffmann, M. Cornelius, J. Morell, M. Fröba, *Angew. Chem. Int. Ed.* **2006**, *45*, 3216–3251.
3. a) T. Aida, K. Tajima, *Angew. Chem. Int. Ed*. **2001**, *40*, 3803–3806; b) Y. Lu, Y. Yang, A. Sellinger, M. Lu, J. Huang, H. Fan, R. Haddad, G. Lopez, A. R. Burns, D. Y. Sasaki, J. Shelnutt, C. J. Brinker, *Nature* **2001**, *410*, 913–917; c) M. Kimura, K. Wada, K. Ohta, K. Hanabusa, H. Shirai, N. Kobayashi, *J. Am. Chem. Soc.* **2001**, *123*, 2438–2439.
4. a) M. Enomoto, A. Kishimura, T. Aida, *J. Am. Chem. Soc.* **2001**, *123*, 5608–5609; b) A. Kishimura, T. Yamashita, T. Aida, *J. Am. Chem. Soc.* **2005**, *127*, 179–183; c) A. Kishimura, T. Yamashita, K. Yamaguchi, T. Aida, *Nature Mater*. **2005**, *4*, 546–549.
5. a). A. Burini, J. P., Jr., Fackler, R. Galassi, B. R. Pietroni, R. J. Staples, *Chem. Commun*. **1998**, 95–96; b). A. Burini, R. Bravi, J. P., Jr., Fackler, R. Galassi, T. A. Grant, M. A. Omary, B. R. Pietroni, R. J. Staples, *Inorg. Chem*. **2000**, *39*, 3158–3165.

Original Publications

1). H. O. Lintang, K. Kinbara, K. Tanaka, T. Yamashita, T. Aida, *Angew. Chem. Int. Ed.* ***Accepted***.
2). H. O. Lintang, K. Kinbara, T. Yamashita, T. Aida, *Small* ***Submitted*** *(*Full Paper*)*.